ACS Catalysis

Research Article

pubs.acs.org/acscatalysis

Unraveling the Catalytic Cycle of Tertiary Phosphine Oxides Reduction with Hydrosiloxane and Ti(O*i*Pr)$_4$ through EPR and ^{29}Si NMR Spectroscopy

Christelle Petit,[†] Evelyne Poli,[‡] Alain Favre-Réguillon,*[,§,∥] Lhoussain Khrouz,[‡] Sandrine Denis-Quanquin,[‡] Laurent Bonneviot,[‡] Gérard Mignani,[⊥] and Marc Lemaire[†]

[†]Laboratoire de Catalyse et de Synthèse Organique, UMR 5246, ICBMS, Université Claude Bernard Lyon 1, 43 bld du 11 Novembre 1918, 69622 Villeurbanne Cedex, France

[‡]ENS Lyon, Laboratoire de Chimie, Groupe Matériaux Hybrides, 46 allée d'Italie, 69364 Lyon cedex 7, France

[§]Laboratoire de Génie des Procédés Catalytiques, UMR 5285, CPE Lyon, 43 bld du 11 Novembre 1918, 69622 Villeurbanne Cedex, France

[∥]Equipe CGP, Département CASER, Conservatoire National des Arts et Métiers, 2 rue Conté, 75003 Paris, France

[⊥]Rhodia Operations, Lyon Research Center, 85, avenue des Frères Perret, BP 62, 69192 Saint-Fons Cedex, France

Supporting Information

ABSTRACT: The reduction of tertiary phosphine oxides using tetramethyldisiloxane (TMDS) as a mild reducing agent and catalytic amount of Ti^{IV} isopropoxide has been studied in detail. An extensive EPR study has revealed the presence of at least five Ti^{III} species, and structures have been proposed. Thus, a single electron transfer (SET) mechanism consisting of a back and forth oxido-reduction of Ti from the IV to the III oxidation state could be proposed. Reduction of Ti^{IV} produces a Si$^{\bullet}$ that undergoes a O^{2-} abstraction from P^{V} compounds leading to P^{III} compounds and Si−O$^{\bullet}$ species. Reoxidation of Ti^{III} by the latter gives silanol species. This mechanism was further probed by ^{29}Si NMR analysis of the reaction mixture as a function of time and by the reduction of optically active P-stereogenic tertiary phosphine oxides. A practical reduction protocol of Ph_3PO with these environmentally benign reagents on a 100 g scale has been developed.

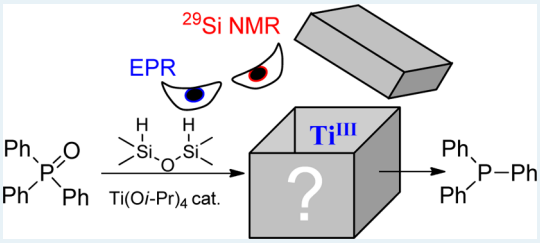

KEYWORDS: *phosphine oxide, reduction, mechanism, silane, EPR*

INTRODUCTION

Tertiary phosphines are an important compound class for metal ligation in transition-metal-catalyzed enantioselective transformations[1,2] or coupling reactions of aryl electrophiles.[3−5] Often, however, these phosphines are prone to oxidation, and a number of reduction strategies were developed.[6] The existing reducing agents, though efficient in producing high yields of desired product, produce undesirable waste products or pose safety problems.[7−11] Finally, silanes[12−16] and a mixture of silanes with a Lewis acid[16−18] remains the reagent of choice for the reduction of phosphine oxides even if some silanes have been demonstrated to be harmful since they generate a dangerous, pyrophoric, and toxic SiH_4 gas.[19]

In recent years, the rediscovery of the reductive abilities of hydrosiloxanes when associated with a catalytic amount of transition metal has renewed interest in using hydrosiloxanes as stoichiometric reductive agents of tertiary and secondary phosphine oxides.[20−26] Indeed, hydrosiloxanes, in comparison to most of the conventional reagents, have many advantages, since they are commercially available, air- and moisture-stable, nonpyrophoric, and soluble in most organic solvents.[19]

Despite this effective procedure being used for decades by numerous research teams, surprisingly little is known about the mechanism of this reduction by hydrosiloxanes as detailed mechanistic studies have not been undertaken.[22] A catalytic cycle has been proposed by Lawrence et al. for the reduction of tertiary phosphine oxides by triethoxysilane involving a titanium hydride-like complex.[17] Recently, we have shown the presence of Ti^{III} in the mixture, which suggests that the reduction of tertiary phosphine oxides may occur via a single electron transfer (SET) mechanism.[24] In this paper, we present complementary studies on the intermediate titanium Ti^{III} species that appears under the reducing action of a TMDS agent and on the mechanism of tertiary phosphine oxides reduction by Ti(O*i*Pr)$_4$ and hydrosiloxanes.

EXPERIMENTAL SECTION

Reduction of Triphenylphosphine Oxide. Triphenylphosphine oxide (390 mg, 1.40 mmol) and methylcyclohexane

Received: October 29, 2012
Revised: May 17, 2013
Published: May 20, 2013

   dx.doi.org/10.1021/cs4002767 | ACS Catal. 2013, 3, 1431−1438

(1.9 mL) were placed in a dry 5 mL round-bottomed flask with a magnetic stirrer. Then, TMDS (620 μL, 3.5 mmol) was added to the reaction vessel followed by $Ti(OiPr)_4$ (80 μL, 0.28 mmol), and the crude mixture was heated to 80 °C. After 14 h, the ^{31}P NMR analysis showed the complete conversion of the starting reagent. The heterogeneous mixture was cooled to 0 °C and filtered over porous glass, and the solid was washed with 4 × 5 mL of pentane. The resulting white solid was dried under vacuum, yielding 365 mg of triphenylphosphine (quantitative yield).

Safety. Unreacted TMDS in the filtrate must be destroyed by the slow addition of a 3 M alcoholic solution of KOH at room temperature. TMDS decomposes on contact with bases, forming hydrogen.

EPR Studies. Methylcyclohexane (5 mL) and TMDS (49 μL, 0.28 mmol) were placed in a dry 10 mL round-bottomed flask with a magnetic stirrer. The flask was capped with a septum, and $Ti(OiPr)_4$ (11.8 μL, 0.04 mmol) was added. The crude mixture was stirred at room temperature until a blue color appeared. Then, 1 mL of the mixture was transferred via syringe into a standard 4 mm quartz dry EPR tube and quickly placed in a small benchtop liquid nitrogen dewar.

RESULTS AND DISCUSSION

Characterization of the Catalytic Species by EPR Spectroscopy. The presence of a singlet state (S = 1/2) at room temperature for the TMDS/$Ti(OiPr)_4$ system had already been noted using EPR spectroscopy.[24] It was concluded that these species correspond to a d^1 Ti^{III} species. On the basis of the saturation test, it was claimed that it could not be an *s* nor *p* type radical.[24] This work is completed here by a low temperature study (Figure 1) and EPR signal simulations in order to identify and quantify the different Ti^{III} species (Figure 2). The signal strongly depends on the concentration of species with the appearance of Ti^{III}−Ti^{III} dimers with S = 1 mixed with Ti^{III}−Ti^{IV} pairs and also Ti^{IV} monomers characterized by S = 1/2. This is reminiscent of the natural tendency of Ti^{IV} alkoxide to oligomerize. In particular, $Ti(PriO)_4$ exhibits a monomer−dimer dynamic equilibrium at room temperature that converts part of the tetrahedral $Ti(PriO)_4$ species into dimers of pentacoordinated Ti^{IV} sharing two μ-OiPr bridging groups, $[Ti^{IV}(OiPr)_4\mu\text{-}(OiPr)_2Ti^{IV}(iPrO)_4]$.[27] Since the radius of the Ti^{III} ion is larger than that of the Ti^{IV} ion, the tendency for dimerization is stronger after reduction favoring the formation of Ti^{III}−Ti^{IV} and Ti^{III}−Ti^{III} pairs at the expense of Ti^{IV}−Ti^{IV} pairs. These pairs are EPR active and were observed in the present system for a high level of reduction and high titanium concentration obtained in optimum condition. Unfortunately, Ti^{III}−Ti^{III} pairs exhibit a complicated and broad signal where hyperfine interactions are not resolved (not reported here). For the sake of simplification and to get better insights on the constitutive Ti^{III} species, it is preferred here to focus on the low concentration conditions where no Ti^{III}−Ti^{III} species can be found. In addition, to avoid a broadening effect, the concentration was lower than in the previous study.[24] As a consequence, the room temperature EPR signal, though similar to that obtained previously, presents a better resolved peak due to less spin−spin interaction known to broaden the signal at high concentrations.[24]

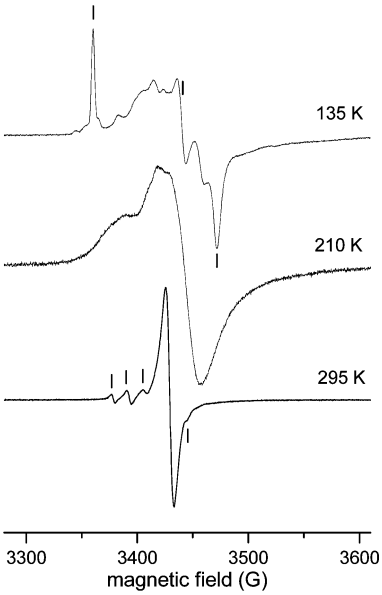

Figure 1. X-band EPR spectrum of the TMDS/$Ti(OiPr)_4$ system as a function of temperature.

At 295 K, instead of two, there are now three well-resolved narrow features pointing upward on the left-hand side of the main peak in the range 3375−3410 G (Figure 1). In addition, the second and third peaks are obviously split into two features so that the triplet is better assigned as two intercalated doublets. The main peak is quasi-symmetric pointing up- and downward centered at 3430 G and a shoulder pointing downward at 3445 G (Figure 1). When the temperature is decreased down to 210 K, the methylcyclohexane (MCH) becomes viscous, slowing down the free rotation of the solvated species, and the signal broadens. A better resolved and much more complex signal appears at 135 K, i.e., below the melting point of MCH (147 K). Indeed, the signal is typical of a powder pattern EPR signal obtained for randomly oriented species in a frozen solvent matrix. Each species is characterized by a complex signal where singularities correspond to the projection of the g and A tensors on the main x, y, and z axes, i.e., g_x, g_y, and g_z and also A_x, A_y, and A_z. Such an analysis requires a simulation, particularly when a mixture of species is at stake, as it appears here according to the number of features on the spectra. There are two distinct narrow peaks at *ca.* 3360 G (upward) and 3470 G (downward) and also a broad one in the middle around 3440 G. The latter results from the superimposition of *ca.* eight secondary lines not regularly spaced one with another. This complexity suggests the presence of more than three species. In addition, the absence of any signal at half field ($g \sim 4$) indicates that there are no S = 1 pairs as planned (vide supra, Figure S1).[28−34] Therefore in the following only S = 1/2 species were considered.

The simulation was performed assuming that the same species could be found at both low and high temperatures. The EPR contributions of the ^{47}Ti (I = 5/2) and ^{49}Ti (I = 7/2) isotopes yielding 6 and 8 line hyperfine structures (hfs) were included in the simulation taking into account their natural abundance, 7.28 and 5.51%, respectively. Though both sets of hfs structures were not fully resolved, they are centered on the g values of the dominating signal of the species with the isotope ^{48}Ti (I = 0), and their intensities are fully imposed by the isotope abundance and the number of lines. Another constraint was exploited to analyze the data knowing that at room temperature the free rotating species exhibit isotropic signals characterized by g_{iso} and A_{iso} split at low temperature into

dx.doi.org/10.1021/cs4002767 | ACS Catal. 2013, 3, 1431−1438

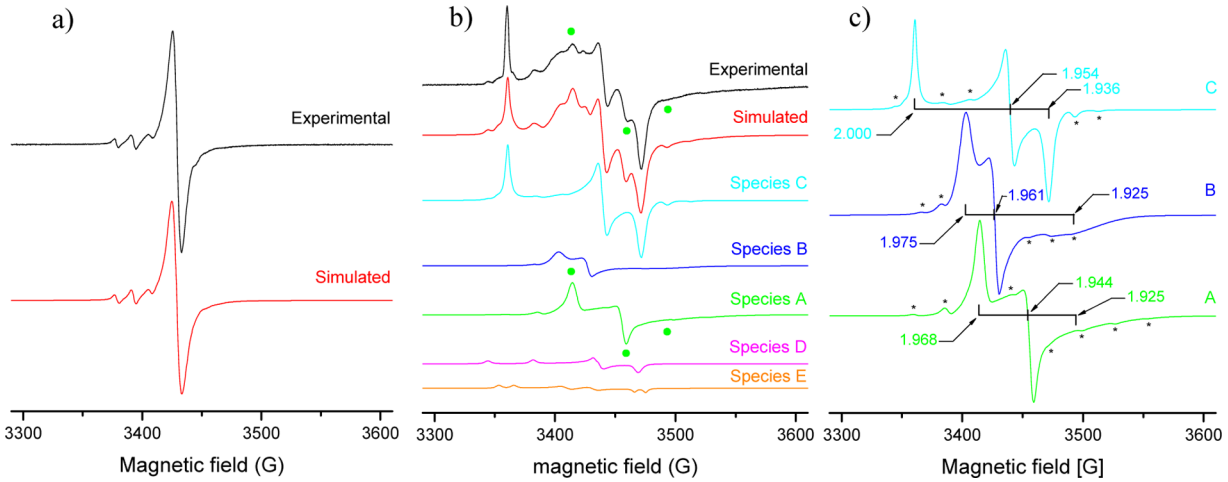

Figure 2. Experimental (black line) and simulated (red line) EPR spectrum of the TMDS/Ti(O*i*Pr)$_4$ system at 295 K (a) and 135 K (b). In b, individual simulated signals A, B, C, D, and E provided the intensity used for the simulation of the experimental spectrum. The green spots stand for the most specific feature of signal A. In c, full scale simulated signals A, B, and C with g_1, g_2, and g_3 assignments and stars pointing the most obvious features of the Ti hfs contributions.

Table 1. EPR Parameters and Relative Concentration of the EPR Active Species from the Simulation of the Experimental Spectrum Measured at 295 K and 135 K (see Table S1 for the Full Set of Parameters)[a]

	295 K				135 K			
species	%	g_{iso}	A_{iso}(Ti)/G	A_{iso}(H)/G	%	g_{av}	A_{av}(Ti)/G	A_{av}(H)/G
A	83	1.961	8.3		25	1.946	8.3	
B	5	1.958	10.0		10	1.953	9.4	
C	5	1.962	6.7		46	1.964	6.4	
D	4	1.986		13.3	6	1.965		13.3
E	3	1.977		13.3	3	1.968		13.3

[a]The accuracy is ±1 on the last digit provided for *g* and *A* values.

several components (g_1, g_2, g_3, A_1, A_2, and A_3) that are much narrower due to longer relaxation times. Usually, apart from a slight effect of the Jahn−Teller distortion, the average values $g_{av} = (g_1 + g_2 + g_3)/3$ and $A_{av} = (A_1 + A_2 + A_3)/3$ should match the room temperature g_{iso} and A_{iso}. This was used as a guide to assign a third component when only two of them were fully resolved.

Then, to reproduce most of the features of the spectra, five different species were necessary and accounted for 94 and 91% of the experimental spectrum at 295 and 135 K, respectively (Table 1 and Figure 2). Reducing the simulation residue would require supplementary signals. This was discarded because of a lack of confidence and low accuracy on such solutions. Among the species, the most intense were simulated from three species characterized by g_{iso} = 1.958, 1.961, and 1.962 that reproduced the slight asymmetrical aspect of the central peak at room temperature. In addition, the little shoulders at the foot of the peak on each side were obtained from different hyperfine splittings (hsf) A_{iso}(Ti) = 10, 8.3, and 6.7 ± 1 G for species denoted as **B**, **A** and **C**, respectively (Table 1). Then, the latter differed mostly from A_{iso}(Ti) hfs (vide infra). The remaining two signals accounting for 4 and 3% of the overall fit were those characterized by a doublet due to the presence of a nearby single proton nucleus (I = 1/2) with a superhyperfine splitting (shfs) constant, A_{iso}(H), of 13.3 and 13.3 G from species and g_{iso} = 1.986 and 1.977 for species denoted as **D** and **E**, respectively. The shift toward g = 2 was consistent with species characterized by a higher crystal field stabilization than in **A**, **B** and **C** species. A_{iso}(H) related to the Fermi contact term corresponded to a spin delocalization of *ca.* 13%.[31] Such doublets were consistent with the shfs of a single proton. It is assigned to a monohydride Ti^{III} species with respect to a series of Ti^{III} dihydride in [Cp*$_2$Ti-(μ-H)$_2$-MgR$_2$] where Cp* = Cp, Me$_x$Cp (x = 0, 3, 4, 5), and R = μ-Cl, μ-Br, μ-OR, Cp, aryl, and butyl, where the spin is delocalized onto two protons leading to an A_{iso}(H) about 2 times smaller, ranging from 5 to 8 G.[32,33]

Accordingly, the simulation of the spectrum registered at 135 K was obtained similarly with three species exhibiting only Ti hfs and two others with only H shfs (Table 1 and Figure 2). At 135 K, all the species exhibited a strong orthorhombicity characteristic of a strong Jahn−Teller distortion typical of d^1 Ti^{III} species, which may explain a slight shift of g_{av} in comparison to g_{iso}. The detailed values of both g and A tensors were provided in the Supporting Information (Table S1) as well as the EPR signal of each simulated species (Figure 2). Once again at 135 K, the hfs of Ti isotopes remained marginal contributions on each side of the main g components (see, for instance, simulated signal A in Figure 2). The relative position of the g tensor components provided the ground state using a first order analysis assuming a pseudoaxial like symmetry: d_{z^2} for species **A** and **C** ($g_2 \sim g_3 \sim g_\perp < g_1 \sim g_\parallel \sim 2$) and $d_{x^2-y^2}$ for species **B** ($g_1 \sim g_2 \sim g_\perp > g_3 \sim g_\parallel$).[31] Furthermore, g_{av} values indicated that the crystal field strength increases from species in the order **A**, B and **C**. The parameters used to solve the structure of each species were based on spectroscopic and chemical criteria as well: (i) g_{av} related to the average crystal field strength and the number of ligands around Ti^{III}, (ii) the ground state provided by the symmetry at the first order (axial

dx.doi.org/10.1021/cs4002767 | *ACS Catal.* 2013, 3, 1431−1438

Scheme 1. Proposed Structures for Species A, B, and C According to EPR Characteristics[a]

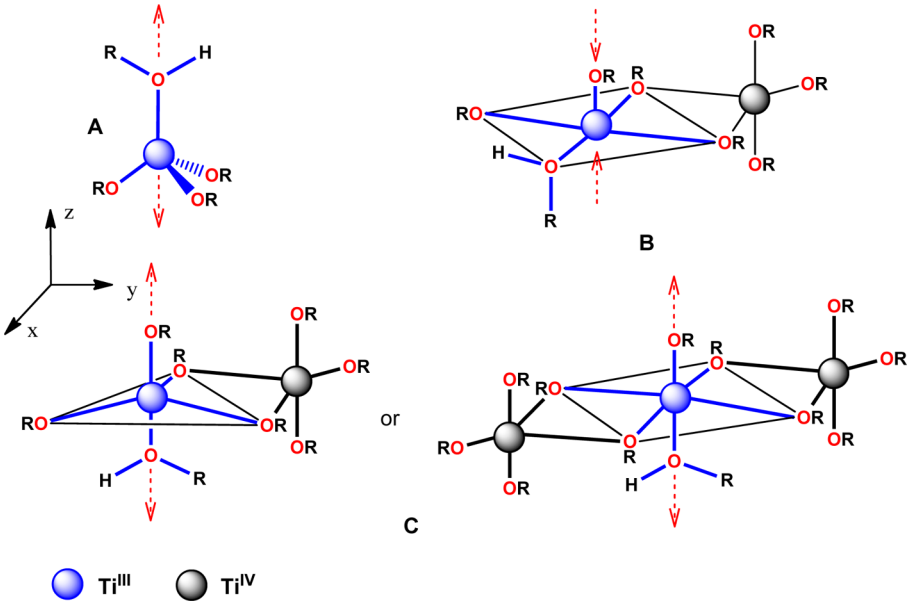

[a]Ti^{III} (blue circle and blue bonds), Ti^{IV} (black circle and black bonds); the latter is smaller and systematically represented in a trigonal bipyramid (tbp) double bridged to Ti^{III} species. Ti^{IV} has no d electron and follows the VSEPR rule. A elongated along the Ti-HOR bond. B has a square pyramidal Ti^{III} with the weaker bonds in the *xy* plane and a Ti-OR bond in the *z* axis. Ti^{III} in C is either pentacoordinated in an elongated tbp symmetry or more likely hexacoordinated in an elongated octahedral environment. See text for species D an E; red arrows depict the first order axial distortion.

approximation) and the strength of the distortion at the second order, (iii) the number of available ligands for Ti in the present system. The latter was limited to four isopropylates, one of them being protonated during the reduction of Ti^{IV} into Ti^{III} species (*vide infra*). Bearing in mind that the alkoxide precursor was a tetrahedral $[Ti^{IV}(OiPr)_4]$, species **A**, characterized by the smallest g_{av} and therefore the weaker crystal field stabilization, was more likely a tetracoordinated $[Ti^{III}(OiPr)_3(iPrOH)]$ or possibly a tricoordinated $[Ti^{III}(OiPr)_3]$ species. Both structures were compatible with a d_{z^2} ground state assuming an elongated tetrahedral symmetry (C_{3v}) for the former and flat triangular symmetry (D_{3h}) for the latter. However, the strong rhombicity of the signal was more compatible with an elongated tetrahedral Ti^{III} species (Scheme 1). For species **A**, the pseudo-axial direction corresponds to the bond with a ligand ROH while the two other directions are necessarily unequivalent due to the presence of the other three ligands RO^- located out of the *xy* plane. The rationale for a stronger crystal field in species **B** and **C** was a higher coordination number, i.e. 5 or 6. A pentacoordinated d^1 species with a $d_{x^2-y^2}$ ground state would be obtained with a compressed pyramid trigonal geometry. A hexacoordinated d^1 species with a d_{z^2} ground state would fit with an elongated octahedral environment for species **C**. Increasing further the coordination number without changing the ratio of metal to ligands will be obtained by oligomerization. A $Ti^{IV}-Ti^{III}-Ti^{IV}$ trimer as exemplified in Scheme 1 is an example that possesses a $Ti^{IV}-Ti^{IV}-Ti^{IV}$ trimer analogue already reported in solution for the tetraethoxytitanium, $[Ti(OEt)_4]$.[34] Alternatively, a pentacoordinated Ti^{III} elongated trigonal bipyramid conformer of species **B** would also fit the ground d_{z^2} ground state but would generate a weaker crystal field. Other types of oligomers or conformers are likely to be formed and may explain the residue of simulation. At this stage of characterization, the assignment of species **C** and the presence of other species remain open. Nonetheless, the formation of the monomeric species **A** was consistently favored at the expense of pairs or higher adducts **B** and **C** at increasing temperatures, suggesting a mixture of species in equilibrium, one with another. Note that there is no resolved proton shfs coupling in species **A**, **B** and **C** despite the presence of the ligand ROH. Indeed such weak coupling was observed using the ENDOR double resonance technique only. Moreover, the pseudo-octahedral $Ti^{III}(H_2O)_6$ species were shown recently to be highly distorted with two energetically close conformations, D_{3d} and C_i, where the unequivalent protons led to the shfs component, also resolved using the double resonance technique.[35]

The relatively small proton shfs of species **E** and **D** precludes the formation of a strong covalent Ti−H bond and would rather fit with a weak Ti−H−Si type of interaction proposed earlier when hydrosilane is in the presence of titanium complexes.[32] Then **E** and **D** will be likely the Lewis acid−base adduct formed between TMDS and **A** and **B**, respectively. These marginal species are not central here to explain the reactivity and will be investigated in a forthcoming paper focusing on the relation between **A**, **B**, **C**, **D** and **E** species.

Structure Analysis of the Reaction Products by ^{29}Si NMR Analysis. To further probe the proposed mechanism, the reduction of Ph_3PO was monitored by an *in situ* ^{29}Si NMR study. The ^{29}Si NMR commonly used $Cr(acac)_3$ as a spin relaxant. ^{29}Si NMR of the crude in $CDCl_3$ using $Cr(acac)_3$ was shown in Figure S3. However, in order to minimize interactions between spin relaxant and deuterated solvents with the intermediate silicone species, ^{29}Si NMR was operated using a coaxial insert filled with D_2O for locking. A DEPT sequence for $^1H-^{29}Si$ coupling was thus used to enhance the signal-to-noise ratio. Shown in Figure 3 are ^{29}Si NMR spectra for four time points (t = 0, 10 min, 4 and 14 h) during the course of the

dx.doi.org/10.1021/cs4002767 | ACS Catal. 2013, 3, 1431−1438

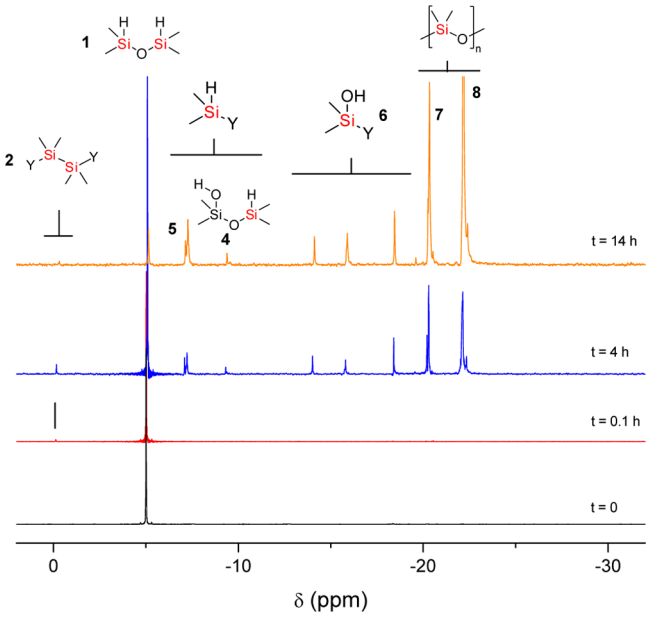

Figure 3. ^{29}Si NMR of the crude reaction mixture of Ph_3PO reduction by TMDS/Ti(O*i*Pr)$_4$.

reaction. Silicon species (Table S2) were identified by comparison with commercial products and literature data.[36,37]

At t = 0, the signal at −5.0 ppm is assigned to TMDS (**1**). At t = 10 min, a small signal could be observed at −0.2 ppm that could be assigned to a disilane species (**2**). It should be emphasized here that no reduction of Ph_3PO could be determined at this point by ^{31}P NMR. Such species could be formed by the coupling of two Si radical centered species **3** (Scheme 2, *vide supra*). The relative signal intensity of **2** increased at t = 4 h, and **2** could be detected at t = 14 h. A higher signal intensity at −0.2 pmm could be observed when using $CDCl_3$ as a solvent, and Cr(acac)$_3$ was used as a spin relaxant at t = 14 h (Figure S3). At t = 4 h, signals between −7 and −7.5 ppm could be attributed to silane species (Table S2, species **4** and **5**). In particular, the signal at −9.3 ppm could be attributed to mono-oxidized TMDS species **5**. Silanol groups between −14 and −19 ppm could be also identified (Table S2, species **6**). It should be emphasized here that the presence of silanol is not expected in the catalytic cycle proposed by Laurence et al.[17,18] Siloxane species (Table S2, species **8** and **9**) between −20 and −23 ppm originating from the condensation of silanol groups were identified in the reaction mixture, and in particular for high Ph_3PO conversion, large signals between −22 and −23 ppm were attributed to cyclic oligomers of siloxane (i.e., cyclomethicone, Table S2, species **8**). All the species with different relative intensities are present in the ^{29}Si NMR spectra of the crude obtained in $CDCl_3$ using Cr(acac)$_3$ as a spin relaxant (Figure S3).

Proposed Mechanism. Following EPR and *in situ* ^{29}Si NMR analysis, an improved catalytic cycle, compared to the catalytic cycle previously published,[24] can be proposed (Scheme 2). The first step consists of one electron reduction[38] of $Ti^{IV}(OiPr)_4$ into a tetracoordinated $[Ti^{III}(OiPr)_3(iPrOH)]$ A by TMDS. A could be stabilized by the formation of species of higher coordination numbers, i.e. **B**, **C**, ... (Scheme 1). This one electron reduction generates a silicon centered radical species **3** that readily reacts with P═O yielding phosphorus radical centered species **9**, which evolved to give desired triphenylphosphine and SiO$^\bullet$ species **10**. Therefore, the balance between species **3** and **10** is a transfer O^{2-} on a Si$^\bullet$ yielding a Si−O bond where oxygen is formally at the −1 oxidation state. Then, the reoxidation of Ti^{III} A by Si−O$^\bullet$ furnished Ti^{IV} and a silanol **4** where oxygen comes back to the −2 oxidation state (Scheme 2). The silanol species **4** and **6** could be identified by ^{29}Si NMR (Figure 3). Incidentally, silicon centered radical species **3** react together, leading to disilane species **2** identified by ^{29}Si NMR

Scheme 2. Proposed Mechanism of Ti(O*i*Pr)$_4$-Catalyzed Reduction of Triphenylphosphine Oxide by Hydrosiloxanes[a]

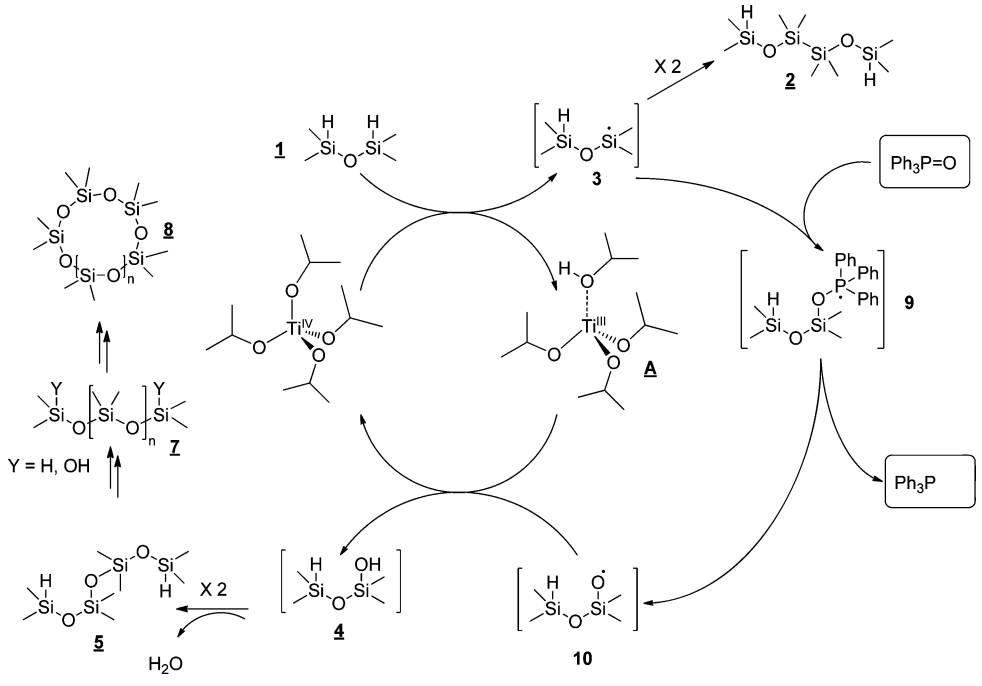

[a]Underline numbers correspond to identifying silicone species by ^{29}Si NMR, and letters correspond to identified titanium species by EPR.

dx.doi.org/10.1021/cs4002767 | *ACS Catal.* 2013, 3, 1431−1438

(Figure 3). The condensation of silanol species is expected to form siloxane species **5**−**8** and water. As already mentioned, an equimolar amount of water is produced as a byproduct, and the use of a drying agent improved the reactivity of the catalytic system.[24] Furthermore, the reduction of Ph_3PO only requires one Si−H function per P═O group[24] whereas two Si−H functions per P═O are needed in Lawrence's mechanism.[17,18]

Reduction of P-Chiral Phosphines Oxides. The proposed catalytic cycle (Scheme 2) involved the formation of phosphorus radical centered species. While the reduction of nonstereogenic phosphine oxides proceeds in high yield,[23,24,26] the stereospecific reduction of pure P-chiral phosphine oxide has never been examined with this system. Thus, the reduction of (*S*,*S*)-DIPAMP oxide (**11**) was studied using standard conditions (Scheme 3). After 24 h at 60 °C, **11** was

Scheme 3. Reduction of Optically Active Tertiary Phosphine Oxides

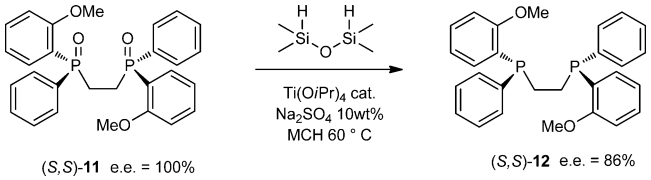

(*S*,*S*)-**11** e.e. = 100% (*S*,*S*)-**12** e.e. = 86%

quantitatively reduced as estimated by ^{31}P NMR, but as expected for the proposed catalytic cycle (Scheme 3), epimerization at phosphorus was observed. An e.e. of 86% was determined by chiral HPLC for DIPAMP **12**. The observed racemization induced by TMDS/$Ti(OiPr)_4$ could occur through a pentacoordinate phosphorus intermediate (species **9** in Scheme 2) which can undergo pseudoracemisation.[6] However, it should be noted that such partial racemization has already been observed during the reduction of P-chirogenic binaphthyl monophosphine oxide using classical methods, such as hydride.[39,40]

Scale Up. On a millimolar scale, the reduction of Ph_3PO proceeded smoothly to completion within 24 h at the temperature of 80 °C, affording triphenylphosphine as the only observable product by HPLC and NMR. The simplicity and efficiency of the transformation led us to pursue the development of a product reduction procedure that would make this methodology adaptable to a 100 g scale.

The first and most critical step in the scale up procedure is to undertake a risk assessment of the reaction. First of all, the thermochemistry of the reduction of Ph_3PO by TMDS/$Ti(OiPr)_4$ was studied using DSC (Figure S4 to S6). Low exothermicity was determined for this reaction, down to 6 J/mol (Figure S7). Then, the *in situ* monitoring of the reaction on a 100 g scale was envisaged. However, Ph_3PO and triphenylphosphine were only slightly soluble in methylcyclohexane. For a concentration up to 0.5 M L^{-1} and 10 wt % of Na_2SO_4,[24] the *in situ* monitoring of the reaction could only be possible using Raman spectroscopy. An analytical method using Raman spectroscopy was thus developed for the monitoring of Ph_3PO, TMDS, and triphenylphosphine concentration. Cyclohexane was used instead of methylcyclohexane in order to simplify Raman spectrum (Figure S8). Raman data were correlated with a ^{31}P NMR analysis of the aliquot as a function of time (Figure 4).

On the 100 g scale and for a concentration of 0.5 M L^{-1} at 60 °C and in the presence of 10 wt % Na_2SO_4, the reaction proceeded smoothly, and a complete conversion was obtained in 14 h. The heterogeneous reaction was cooled, and triphenylphosphine was recovered by filtration using a Buchner funnel. The obtained solid was washed with pentane to remove silicone derivatives, and triphenylphosphine was obtained with a quantitative yield after recrystallization from acetone. The filtrate was cooled to 0 °C, and a 3 M alcoholic solution of KOH was carefully added under vigorous stirring to destroy the remaining Si−H functional group.

CONCLUSION

In summary, the reduction of Ph_3PO by the TMDS/$Ti(OiPr)_4$ system was studied in detail for the first time, and a mechanism involving a single electron transfer was proposed. The catalytic species that involves a reduced state of titanium in the initiation

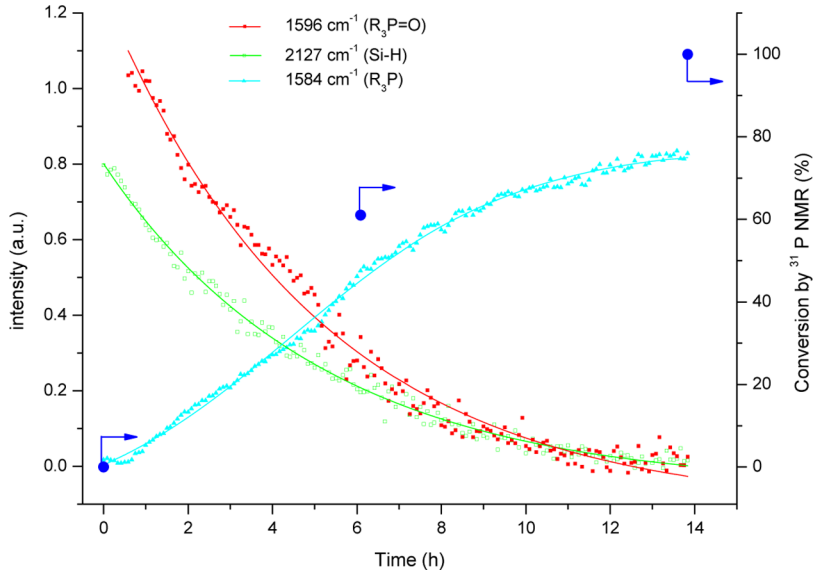

Figure 4. Monitoring of Ph_3PO reduction on a 100 g scale using Raman spectroscopy. Experimental conditions: TMDS (Si−H/P═O = 2.1), $Ti(OiPr)_4$ 10% cat., Na_2SO_4 (10 wt %), cyclohexane, 60 °C.

dx.doi.org/10.1021/cs4002767 | *ACS Catal.* 2013, 3, 1431−1438

step was investigated using EPR investigations at different temperatures. The spectra exhibit a mixture of species characteristic of Ti^{III}, $S = 1/2$, species and $Ti^{III}-Ti^{III}$, $S = 1$ pairs. The spin $S = 1$ pairs produce a broad signal that could not be isolated from the $S = 1/2$ systems. Nonetheless, at a low reduction level, the $S = 1$ system disappears, yielding a mixture of five different $S = 1/2$ species. Both room temperature and low temperature (frozen matrix) spectra were simulated providing some insights from the g and A tensors on the symmetry and coordination number of the Ti^{III} center of each species. The rationale for such a variety of species is related to the tendency of Ti^{IV} alkoxides to dimerize, a phenomenon more favorable for Ti^{III} ions that have a larger ionic radius than Ti^{IV} ions. Then, monomeric tetrahedral Ti^{III} species, $Ti^{III}-Ti^{IV}$ pairs, and eventually $Ti^{IV}-Ti^{III}-Ti^{IV}$ trimers are likely to coexist under partial reduction and were tentatively assigned. Indeed, the dominating species at room temperature is the elongated tetrahedral Ti^{III} species A (~ 80%) that is coordinatively unsaturated and preferably associated with the catalytic activity.

The proposed mechanism is in agreement with the *in situ* ^{29}Si NMR analysis of the silicon based intermediate, the stoichiometry of the reaction, EPR studies, and partial racemization obtained with stereogenic phosphine oxides. The mechanism is based on a back and forth oxido-reduction of Ti from IV to III oxidation state.[38] First, titanium(IV) acts as a one-electron oxidation species on SiH producing $Si^{\bullet}$. Second, the so-obtained titanium(III) species reduces the $SiO^{\bullet}$ intermediate into a silanol species. The reduction of tertiary phosphine oxides thus consists of a transfer of O^{2-} species on a $Si^{\bullet}$ yielding $SiO^{\bullet}$ where oxygen is formally at the oxidation state −1. Moreover, a reduction of Ph_3PO on a 100 g scale was described. These conditions may be attractive as a general way to reduce tertiary phosphine oxides. This improved method involved the following characteristic features: (1) An air- and moisture-stable hydrosiloxane reagent was used as a hydride source. (2) Water-insoluble "process friendly" solvents such as toluene, methylcyclohexane, and cyclohexane were used as solvents. (3) Crystals of triphenylphosphine were obtained directly with a straightforward workup. (4) Treatment of the waste stream by potassium hydroxide gave inert TiO_2 and siloxanes. (5) This reaction is general.[23−26]

■ ASSOCIATED CONTENT

Supporting Information

Synthesis and characterization of the products; simulation parameters of the EPR signal spectra at 135 K; experimental and simulated EPR spectrum at 295 K; ^{29}Si NMR analysis of the reactions products; DSC analysis; Raman spectra of individual species. This material is available free of charge via the Internet at http://pubs.acs.org.

■ AUTHOR INFORMATION

Corresponding Author

*E-mail: afr@lgpc.cpe.fr (A. F.-R.).

Notes

The authors declare no competing financial interest.

■ ACKNOWLEDGMENTS

This work was supported by Rhodia Operations through a Ph.D. grant to C.P. We thank Dr. Nicolas Capelle, Jean Louis Gustin, and Serge Henrot from Rhodia Operations for assistance with ^{29}Si NMR, DSC, and RAMAN spectroscopy.

■ REFERENCES

(1) Jacobsen, E. N.; Pfaltz, A.; Yamamoto, H. *Comprehensive asymmetric catalysis*; Springer-Verlag GmbH: Berlin, 1999.
(2) Ojima, I. *Catalytic asymmetric synthesis*; Wiley-VCH: New York, 2000.
(3) Diederich, F.; Stang, P. J. *Metal-catalyzed cross-coupling reactions*; Wiley-VCH: Weinheim, Germany, 1997.
(4) Tsuji, J. *Palladium reagents and catalysts*; Wiley & Sons: Chichester, U. K., 2004.
(5) Beller, M.; Bolm, C. *Transition metals for organic synthesis*. Wiley-VCH: Weinheim, Germany, 2004.
(6) Engel, R. *Handbook of organophosphorus chemistry*; Engel, R., Ed.; Marcel Dekker: New York, 1992.
(7) Imamoto, T.; Kikuchi, S.-I.; Miura, T.; Wada, Y. *Org. Lett.* **2001**, *3*, 87−90.
(8) Imamoto, T.; Takeyama, T.; Kusumoto, T. *Chem. Lett.* **1985**, 1491−1492.
(9) Bootle-Wilbraham, A.; Head, S.; Longstaff, J.; Wyatt, P. *Tetrahedron Lett.* **1999**, *40*, 5267−5270.
(10) Busacca, C. A.; Raju, R.; Grinberg, N.; Haddad, N.; James-Jones, P.; Lee, H.; Lorenz, J. C.; Saha, A.; Senanayake, C. H. *J. Org. Chem.* **2008**, *73*, 1524−1531.
(11) Rajendran, K. V.; Gilheany, D. G. *Chem. Commun.* **2012**, *48*, 817−819.
(12) Fritzsche, H.; Hasserodt, U.; Korte, F.; Friese, G.; Adrian, K.; Arenz, H. J. *Chem. Ber.* **1964**, *97*, 1988−1993.
(13) Horner, L.; Balzer, W. D. *Tetrahedron Lett.* **1965**, 1157−1162.
(14) Naumann, K.; Zon, G.; Mislow, K. *J. Am. Chem. Soc.* **1969**, *91*, 2788−2789.
(15) Krenske, E. H. *J. Org. Chem.* **2012**, *77*, 1−4.
(16) *Organophosphorus Chemistry Series*; Allen, D. W., Tebby, J. C., Eds.; Royal Society of Chemistry Cambridge: Cambridge, U. K.; pp 1970−2012.
(17) Coumbe, T.; Lawrence, N. J.; Muhammad, F. *Tetrahedron Lett.* **1994**, *35*, 625−628.
(18) Lawrence, N. J.; Drew, M. D.; Bushell, S. M. *J. Chem. Soc., Perkin Trans. 1* **1999**, 3381−3391.
(19) Wells, A. S. *Org. Process Res. Dev.* **2010**, *14*, 484−484.
(20) Li, Y.; Das, S.; Zhou, S.; Junge, K.; Beller, M. *J. Am. Chem. Soc.* **2012**, *134*, 9727−9732.
(21) Li, Y.; Lu, L.-Q.; Das, S.; Pisiewicz, S.; Junge, K.; Beller, M. *J. Am. Chem. Soc.* **2012**, *134*, 18325−18329.
(22) Harris, J. R.; Haynes, M. T.; Thomas, A. M.; Woerpel, K. A. *J. Org. Chem.* **2010**, *75*, 5083−5091.
(23) Berthod, M.; Favre-Reguillon, A.; Mohamad, J.; Mignani, G.; Docherty, G.; Lemaire, M. *Synlett* **2007**, 1545−1548.
(24) Petit, C.; Favre-Reguillon, A.; Albela, B. l.; Bonneviot, L.; Mignani, G.; Lemaire, M. *Organometallics* **2009**, *28*, 6379−6382.
(25) Petit, C.; Favre-Reguillon, A.; Mignani, G.; Lemaire, M. *Green Chem.* **2010**, *12*, 326−330.
(26) Dayoub, W.; Favre-Reguillon, A.; Berthod, M.; Jeanneau, E.; Mignani, G.; Lemaire, M. *Eur. J. Org. Chem.* **2012**, 3074−3078.
(27) Babonneau, F.; Doeuff, S.; Leaustic, A.; Sanchez, C.; Cartier, C.; Verdaguer, M. *Inorg. Chem.* **1988**, *27*, 3166−3172.
(28) Samuel, E.; Harrod, J. F.; Gourier, D.; Dromzee, Y.; Robert, F.; Jeannin, Y. *Inorg. Chem.* **1992**, *31*, 3252−3259.
(29) Lukens, W. W.; Andersen, R. A. *Inorg. Chem.* **1995**, *34*, 3440−3443.
(30) Horácek, M.; Gyepes, R.; Císarová, I.; Kubista, J.; Pinkas, J.; Mach, K. *J. Organomet. Chem.* **2010**, *695*, 2338−2344.
(31) Weil, J. A.; Bolton, J. R. *Electron paramagnetic resonance: elementary theory and practical applications*; Wiley: New York, 2007.
(32) Gyepes, R.; Hiller, J.; Thewalt, U.; Polasek, M.; Sindelar, P.; Mach, K. *J. Organomet. Chem.* **1996**, *516*, 177−185.
(33) Horacek, M.; Cisarova, I.; Cejka, J.; Karban, J.; Petrusova, L.; Mach, K. *J. Organomet. Chem.* **1999**, *577*, 103−112.
(34) Russo, W. R.; Nelson, W. H. *J. Am. Chem. Soc.* **1970**, *92*, 1521−1526.

(35) Maurelli, S.; Livraghi, S.; Chiesa, M.; Giamello, E.; Van Doorslaer, S.; Di Valentin, C.; Pacchioni, G. *Inorg. Chem.* **2011**, *50*, 2385−2394.
(36) Kintzinger, J. P.; Marsmann, H. *NMR Basic Principles and Progress: Oxygen-17 and Silicon-29*; Springer-Verlag: Berlin, 1981.
(37) Gupta, R. R.; Lechner, M. D.; Marsmann, H.; Mikhova, B.; Uhlig, F. *Chemical shifts and coupling constants for Silicon-29*; Springer: Berlin, 2008.
(38) Praneeth, V. K. K.; Ringenberg, M. R.; Ward, T. R. *Angew. Chem., Int. Ed. Engl.* **2012**, *51*, 10228−10234.
(39) Higham, L. J.; Clarke, E. F.; Mueller-Bunz, H.; Gilheany, D. G. *J. Organomet. Chem.* **2005**, *690*, 211−219.
(40) Kerrigan, N. J.; Dunne, E. C.; Cunningham, D.; McArdle, P.; Gilligan, K.; Gilheany, D. G. *Tetrahedron Lett.* **2003**, *44*, 8461−8465.